Interactions of Nanosized Al_2O_3 and ZnO with Poly(ethylene oxide)−NaSCN Polymer Electrolytes

Hucheng Zhang, Jianji Wang,* Honghe Zheng, Kelei Zhuo, and Yang Zhao

School of Chemistry & Environmental Science, Henan Normal University, Xinxiang, Henan 453002, People's Republic of China

Received: September 14, 2004; In Final Form: November 27, 2004

The effect of nanosized Al_2O_3/ZnO fillers on the interactions in PEO−NaSCN polymer electrolytes has been studied by FT-IR, XRD, and DTA measurements. The experimental results are discussed according to the grain boundary effect, the principle of Lewis acid−base, and epitaxial effect. It is shown that the hard Lewis acid centers on the surface of Al_2O_3 exhibit strong interactions with ether oxygens in PEO, even with ether oxygens that coordinated to Na^+. Therefore, the modes of the interaction of Al_2O_3 with PEO−NaSCN electrolytes are dependent on the salt content. Al_2O_3 cannot influence the ionic association in $P(EO)_8NaSCN$ electrolyte, but do reduce significantly the solvating ability of PEO toward NaSCN in $P(EO)_{60}NaSCN$ electrolyte. However, NaSCN in $P(EO)_{20}NaSCN-30\%Al_2O_3$ nanocomposite appears as a state that resembles the situation of NaSCN in PEO amorphous phase. In contrast with Al_2O_3, the epitaxial effect of ZnO is not found in the interested systems where only weaker interaction is observed between ZnO and ether oxygen, and the modes of interaction of ZnO with PEO−NaSCN electrolytes are hardly related to the salt content. In addition, the soft Lewis acid groups on ZnO surface exhibit stronger complexation with SCN^- in PEO−NaSCN electrolytes, and both can form the complex anion $ZnO\cdots SCN^-$.

1. Introduction

Solid polymer electrolytes (SPEs) have become the subject of intensive study because they are envisaged to be the most suitable candidates for replacing the liquid electrolytes used in some electrochemical devices.[1−4] Poly(ethylene oxide) (PEO) is a successful host to prepare SPEs and has been investigated extensively due to its ability to dissolve salt well and proper structure to support ion transport. However, the presence of high crystallinity in PEO-based SPEs impedes the ion transport by limiting the segmental motion and results in the quite low conductivity at ambient temperatures. Therefore, various methods have been developed to increase the volume fraction of the PEO amorphous phase and to improve the conductivity of the SPEs.[4−9] Nanocomposite polymer electrolytes, which are prepared by the addition of nanosized ceramic fillers (such as SiO_2, Al_2O_3, MgO, ZrO_2, γ-$LiAlO_2$, TiO_2, $BaTiO_3$, $LiTaO_3$, and ZnO)[10−13] into PEO-based SPEs, have attracted considerable attention because they provide many advantages over those prepared by other methods. It has been shown that the use of inorganic fillers not only decreases the crystallinity of PEO and enhances the ionic conductivity, but also improves mechanical stability and extends the thermal stability range of PEO-based electrolytes. In addition, an improved stability of the electrode−electrolyte interface and an enhancement of the cation transport number have also been reported, which are the important factors controlling the performance of batteries.

Depending on the type, particle size, and content of the used fillers, the conductivity of PEO-based nanocomposite polymer electrolytes can be enhanced up to 2 orders of magnitude at room temperature. It is well known that the crucial role in enhanced properties of SPE is the interface between nano-filler and polymer,[9] and several models[14,15] have been established to explain the effect of nanosized filler on the SPE properties. However, the mechanism by which the electrochemical properties are improved is still not fully understood. Because SPE properties strongly depend on the interactions among PEO, salt, and ceramic filler, the studies of interactions are essential to insight into the structure and mechanism of ion transport in nanocomposites and may especially serve the purpose for the development of novel SPEs. In this work, nanocomposite polymer electrolytes prepared by the addition of nanosized Al_2O_3 or ZnO into PEO−NaSCN electrolytes have been investigated using Fourier transform-infrared (FT-IR), differential thermal analysis (DTA), and X-ray diffraction (XRD) measurements. The goal of this work is to analyze the effects of nanosized filler and NaSCN content on interactions and to discuss the roles played by filler in nanocomposite polymer electrolyte, in an attempt to predict the improvements in the ionic conductivity and the cation transport number. Moreover, the interactions of Al_2O_3 with PEO−NaSCN electrolytes are also compared to those of ZnO.

2. Experimental Section

PEO ($M_W = 6 \times 10^6$) was a special gift from Liansheng Co. and was dried under vacuum at ~60 °C for 24 h to remove traces of water in the sample. NaSCN (reagent grades, 99.0%) was twice recrystallized in anhydrous ethanol and was dried under vacuum at 80 °C for 24 h. γ-Al_2O_3 and ZnO (Mingri Co.) are in the same purity of 99.5% and have grain sizes of 15 and 20 nm, respectively, according to the manufacture's specifications. The two types of ceramic filler were vacuum-dried at 170 °C for 24 h prior to use. PEO and given amounts of NaSCN and Al_2O_3/ZnO were mixed with anhydrous acetonitrile (99.9%) and stirred vigorously at room temperature for 24 h until a homogeneous solution was formed. The resulting

* Corresponding author. Tel.: +86-373-3325996. Fax: +86-373-3326544. E-mail: jwang@henannu.edu.cn.

10.1021/jp045838d CCC: $30.25
Published on Web 01/25/2005

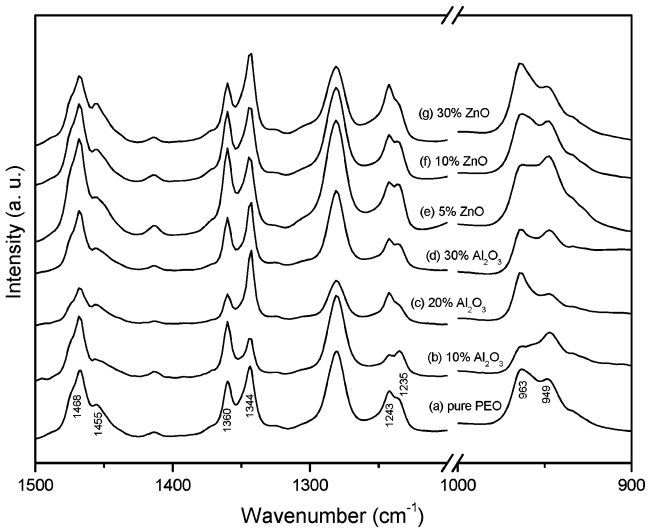

Figure 1. FT-IR spectra of PEO in PEO−Al_2O_3/ZnO mixtures in the 1500−900 cm^{-1} region. Contents for each curve are given as wt % of Al_2O_3/ZnO in PEO.

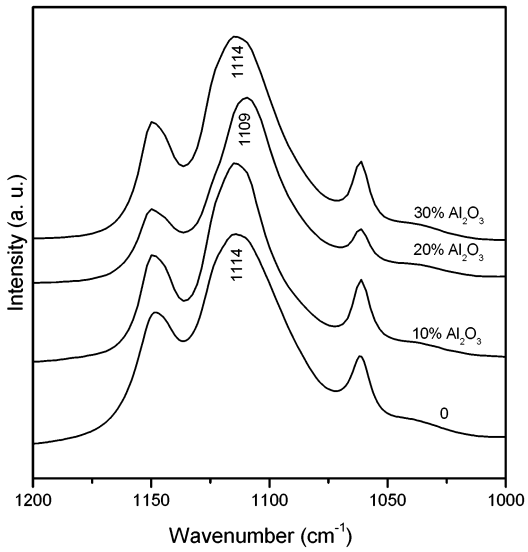

Figure 2. FT-IR spectra of PEO in PEO−Al_2O_3 mixtures in the 1200−1000 cm^{-1} region. Contents for each curve are given as wt % of Al_2O_3 in PEO.

solution was cast on a Teflon plate and allowed to evaporate slowly inside a desiccator. The films thus obtained were dried at 80 °C in a vacuum for 24 h. Before measurements, all heated samples were cooled at room temperature for more than 6 h for the purpose of eliminating completely the effect of the PEO crystallization process on the experimental results. The composition of SPEs is represented as $P(EO)_nNaSCN-y\%$, where n refers to the molar ratio of the ethylene oxide repeating unit and the salt, and y% is the weight percent (wt %) of filler in PEO present.

For infrared measurements, the gelatinous polymer solution was cast on a KBr window and vacuum-dried at 80 °C for 2 h, and the infrared absorption spectrum was recorded at room temperature on a computer-interfaced Bio-Rad Digilab FTS-40 FT-IR spectrometer in the range of 4000−400 cm^{-1} with a resolution of 2 cm^{-1}. Dry N_2 purging gas was used to exclude the infrared active H_2O and CO_2 in the atmosphere from the sample chamber.

The melting temperatures of crystalline PEO in nanocomposite samples were determined by DTA measurements, which were performed under N_2 purging gas using the Shimadzu DT-40 thermal analyzer. Samples were loaded in sealed aluminum pans, and DTA thermograms were recorded at a heating rate of 10 °C min^{-1}. The X-ray diffraction experiments of composite films were conducted on a Bruker D_8 X-ray diffractometer with Cu Kα radiation and were performed at 40 kV and 150 mA with a scanning rate of 2 deg min^{-1}.

3. Results and Discussion

3.1. Interactions of PEO with Al_2O_3/ZnO. Figure 1a shows the FT-IR spectrum of pure PEO in the range of 1500−900 cm^{-1}. The bands at 949 and 963 cm^{-1} are assigned to the CH_2 rocking modes, the bands at 1235 and 1243 cm^{-1} are attributed to the CH_2 twisting modes, and the bands at 1343 and 1360 cm^{-1} are ascribed to the CH_2 wagging modes.[16,17] Because these bands change sensitively with the macromolecular conformations and crystallinity, the analysis of CH_2 vibrational bands allows us to reveal the change of the gauche/trans conformer ratio in PEO conformations. It has been reported that the relative intensities of the bands at 963, 1243, and 1344 cm^{-1} increase with respect to those of the bands at 949, 1235, and 1360 cm^{-1}, and the COC stretching mode for 1114 cm^{-1} in pure PEO shifts to 1109 cm^{-1} in PEO−NaSCN complex due to the complexation of ether oxygen with Na^+ of NaSCN.[18,19] These changes are in good agreement with the spectral behavior observed for PEO−alkaline metal salt complexes[20−22] and are associated with the increase of the number of gauche conformers along the PEO chain.

Contrary to the spectral observations in PEO−NaSCN complexes, it is found that the relative intensities of the bands at 949, 1235, and 1360 cm^{-1} increase with respect to those of the bands at 963, 1243, and 1344 cm^{-1} with increasing Al_2O_3 content in PEO up to 10%, whereas no significant change is observed for the COC stretching mode as shown in Figures 1b and 2. It is possible that the spectral changes result from the grain boundary effect of nanosized Al_2O_3, which decreases the gauche/trans conformer ratio along the PEO chain. Along with the increase of trans conformer, PEO molecular chains undergo the transition from order to disorder and take the conformations that are very similar to those of low-molecular-weight PEO. Moreover, the PEO crystalline phase, to a certain extent, goes to disruption in the presence of Al_2O_3. However, with the Al_2O_3 content increased further, the relative intensities of the bands at 949, 1235, and 1360 cm^{-1} decrease, but those of the bands at 963, 1243, and 1344 cm^{-1} increase, and the band of the COC stretching mode shifts from 1114 cm^{-1} in pure PEO to 1109 cm^{-1} in PEO−20% Al_2O_3 mixture. These spectral data are similar to those observed in the complexes of PEO−alkaline metal salt, suggesting the complexation of Al_2O_3 with PEO occurs in PEO−Al_2O_3 mixtures. According to the Lewis acid−base principle which has been used well to predict the interactions between PEO and nanosized fillers,[17,13−25] the complexation results from the interactions of Lewis acidic sites on Al_2O_3 surface with Lewis base centers of ether oxygen in PEO. Although the Lewis acid−base interactions can also lead to the reduction of PEO crystallinity and the transformation of polymeric conformations, the interactions, which are different from the grain boundary effect, increase the gauche conformer in PEO molecules and restrict the flexibility of PEO chains. Surprisingly, when the Al_2O_3 content reaches 30%, the PEO spectrum is roughly the same as that of pure PEO. Because both Al_2O_3 and PEO interact strongly and the agglomeration of Al_2O_3 in PEO is not found experimentally up to the content of 30% Al_2O_3, the phenomenon is possibly a result of PEO

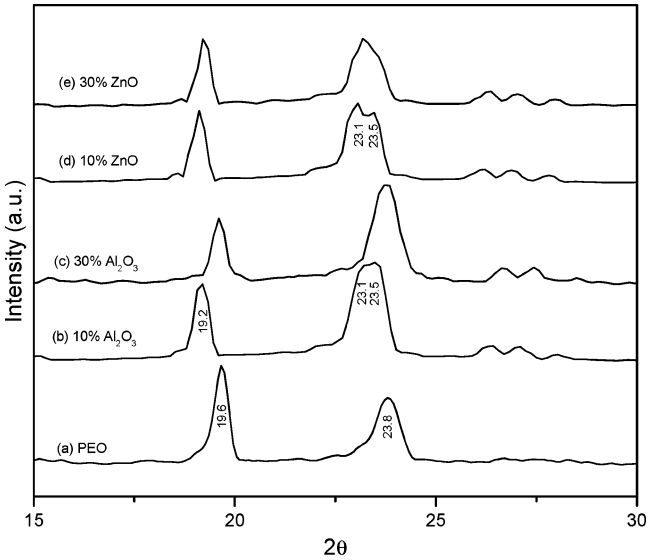

Figure 3. XRD patterns of PEO−Al_2O_3/ZnO mixtures. Contents for each curve are given as wt % of Al_2O_3/ZnO in PEO.

crystallization and is caused by the epitaxial effect of Al_2O_3.[23,26] This fact can be substantiated further by XRD and DTA measurements.

Figure 3a shows the XRD pattern of pure PEO. There are two intense peaks that appear at $2\theta = 19.6°$ and 23.8°, respectively. The Bragg reflection lines are in agreement with those reported by Kulkarni.[27] With the addition of Al_2O_3 into PEO, the two intense peaks shift slightly toward low 2θ and become broadened as shown in Figure 3b, indicating the reduction of PEO long-range crystalline order and the increase of amorphous phase volume fraction. In addition, it is also found that the peak at 23.8° exhibits two peaks at 23.1° and 23.5° when it shifts toward low 2θ. This phenomenon is possibly caused by the interactions of the inorganic filler with PEO, which results in the formation of two discrete phases in PEO−10%Al_2O_3: one on Al_2O_3 surface and the other at Al_2O_3 vicinity. When the Al_2O_3 content reaches 30%, the two intense peaks in the XRD pattern appear at the exact same 2θ as pure PEO, indicating that the excessive Al_2O_3 promotes PEO crystallization due to heterogeneous nucleation of the inorganic filler.[28,29] However, the relative intensities of both peaks are different from those of pure PEO and indicate that the PEO crystal induced by Al_2O_3 is different from that formed in pure polymer. This is consistent with the fact that the surface of inorganic fillers, in some cases, can promote polymers to grow a different crystal phase.[26] Figure 4 presents the DTA thermograms of PEO−Al_2O_3/ZnO mixtures. It is shown that the melting temperature (63.4 °C) of crystalline PEO in the PEO−30% Al_2O_3 mixture is a little higher than that (61.8 °C) in the PEO−10% Al_2O_3 mixture, but lower than that (66.8 °C) of pure PEO. These data confirm that the PEO crystallization behavior in the presence of Al_2O_3 is different from that in pure PEO. It is possible that the PEO crystal produced by Al_2O_3 nucleation takes more dispersed and tiny characteristics.

Figure 1e−g shows the IR spectra of CH_2 vibrational modes of PEO in PEO−ZnO mixtures in the range of 1500−900 cm^{-1}. With the increase of ZnO content, spectral changes of PEO are found to be similar to those reported in PEO−Al_2O_3 mixtures. These facts may be ascribed to the grain boundary effect and the interactions of Lewis acidic sites on ZnO surface with Lewis base centers of the ether oxygen in PEO. However, when the interactions of Lewis acid−base type become significant, the nano-filler content in the ZnO−PEO mixture is more than 5%,

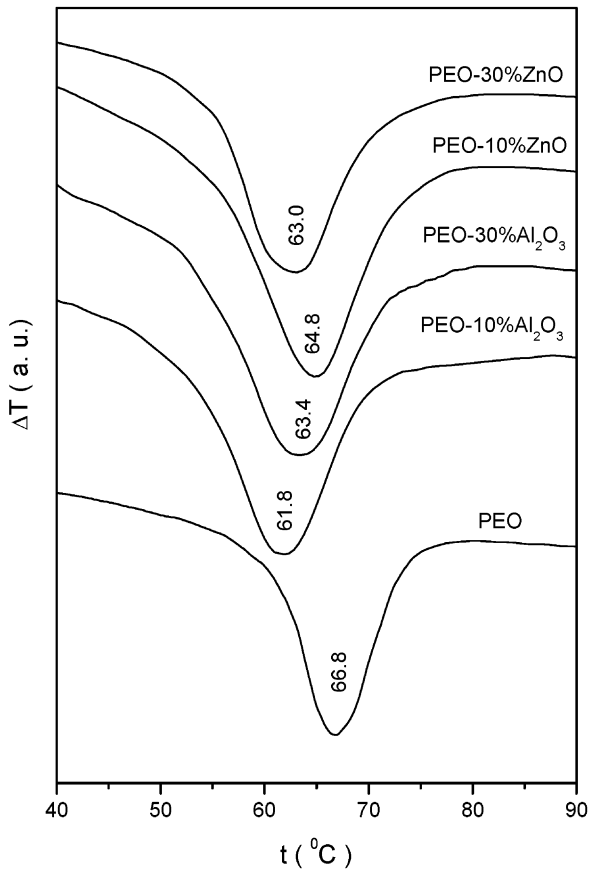

Figure 4. DTA thermograms of PEO−Al_2O_3/ZnO mixtures.

which is less than that observed in PEO−Al_2O_3 mixtures. Moreover, the PEO crystallization in the ZnO−PEO mixture is not found up to the ZnO content of 30%. Obviously, the interactions between ZnO and PEO are weaker than those between Al_2O_3 and PEO. Therefore, ZnO exhibits the poor compatibility with PEO and the poor ability to transform PEO from crystalline to amorphous phase. Figure 3d and e shows the XRD patterns of PEO−ZnO mixtures. Like PEO−Al_2O_3 mixtures, it is observed that the two intense peaks of PEO in the mixtures shift to low 2θ with the addition of ZnO into PEO. The peak at $2\theta = 23.8°$ becomes broadened and consists of the peaks at 23.1° and 23.5° due to the interactions of ZnO with PEO. DTA experiments show that the melting temperature of crystalline PEO in PEO−ZnO mixtures has a tendency to decrease with increasing ZnO content and reaches 63.0 °C in PEO−30%ZnO mixture as shown in Figure 4. Although ZnO can also interact with PEO through the grain boundary effect and Lewis acid−base sites, the very weak interactions of ZnO with PEO, when compared with Al_2O_3−PEO mixtures, suggest that Lewis acidic centers on ZnO surface are softer than those on Al_2O_3 surface because the ether oxygen is a Lewis hard base.

3.2. Interactions of Al_2O_3 with PEO−NaSCN Electrolytes. SCN^- belongs to point group symmetry $C_{\infty v}$ and has three vibrational modes that are associated with the CN stretching, the CS stretching, and the doubly degenerate SCN^- bending modes, respectively. The CN stretching modes have high absorption intensity, high sensitivity to its ionization states, and little overlap with the FT-IR spectrum of PEO. Therefore, SCN^- is a good candidate for studying ion association in PEO-based SPEs by vibrational spectroscopy. The FT-IR spectrum of the CN stretching modes in PEO−NaSCN electrolytes appears as one envelope in the region of 2150−2000 cm^{-1}. To investigate the behavior of ion association of NaSCN in PEO, this envelope

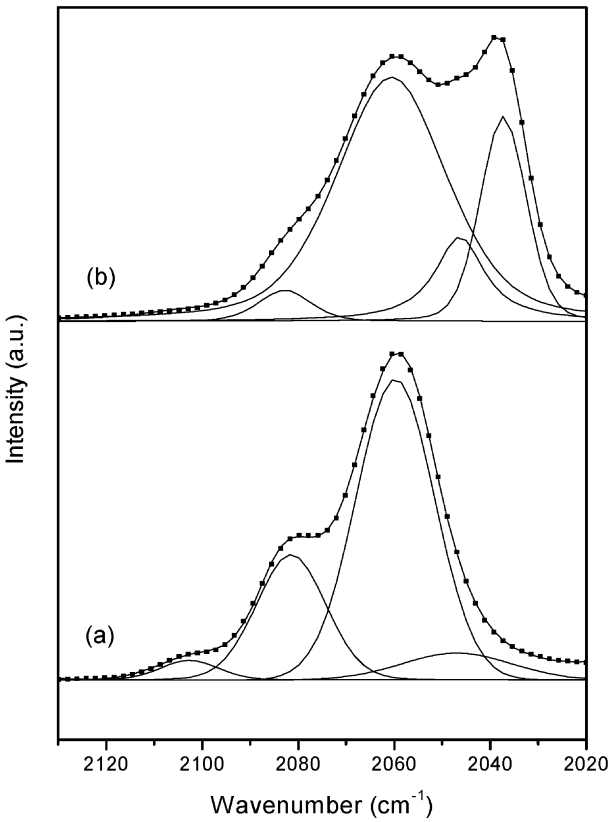

Figure 5. Deconvolution of FT-IR spectra for SCN^- in PEO−NaSCN electrolytes in the region of 2130−2020 cm^{-1}: (a) $P(EO)_{60}NaSCN$, (b) $P(EO)_{20}NaSCN$.

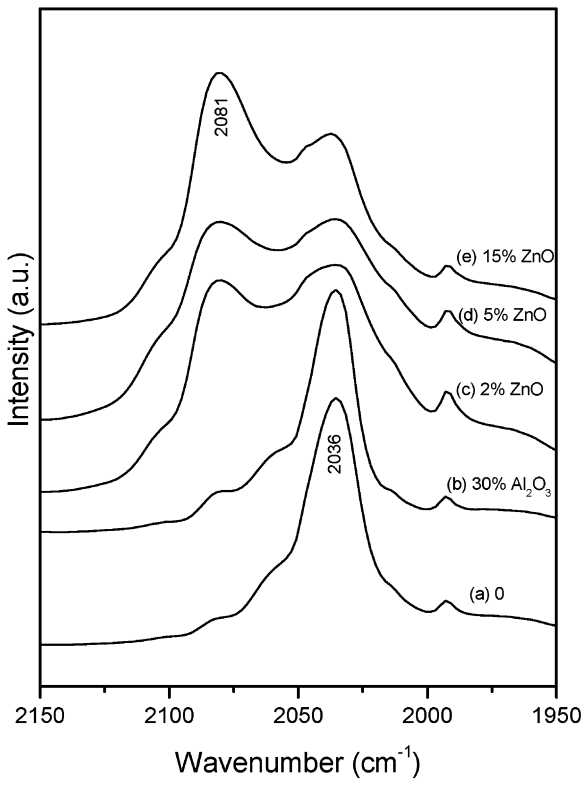

Figure 6. FT-IR spectra of SCN^- in $P(EO)_8$−NaSCN−Al_2O_3/ZnO nanocomposite electrolytes in the 2150−1950 cm^{-1} region. Contents for each curve are given as wt % of Al_2O_3/ZnO in PEO.

is curve-fit to a straight baseline and one Gaussian−Lorentzian product function for each band using the Win-IR software, a program of Bio-Rad spectrometer. As seen from the curve-fitting results shown in Figure 5, the CN stretching modes in the region of 2130−2020 cm^{-1} consist of four bands when the NaSCN content is less than that in $P(EO)_{20}NaSCN$ electrolyte. The band at ∼2047 cm^{-1} is assigned to spectroscopically free SCN^- and solvent-separated ion-pairs,[30,31] the band at ∼2060 cm^{-1} is ascribed to the contact ion-pairs and solvent-separated dimers,[32] and the bands at ∼2080 and 2103 cm^{-1} are attributed to the triple ion and the higher ion aggregations, respectively.[32,33] With the increase of NaSCN content in PEO, a new band at 2037 cm^{-1} sprouts out at the expense of the bands at 2047 and 2060 cm^{-1} as shown in Figure 5b. The band at 2037 cm^{-1} is an indication of the formation of crystalline complex $P(EO)_3$-NaSCN and is associated with the CN stretching vibration in $P(EO)_3NaSCN$, which has been discussed in detail in our previous papers.[18,19]

The ambient property of SCN^- makes it possible to complex metal ions through its nitrogen or sulfur atoms and to form N- or S-bonded or bridge complexes, depending on the type of metals, the nature of the ligands, and the steric effects. Therefore, the interactions of Lewis acid−base type in PEO−NaSCN−Al_2O_3 nanocomposite electrolytes involve the ether oxygen, the Lewis acid site on the Al_2O_3 surface, the Na^+, the nitrogen, and the sulfur of SCN^-. Because Na^+ is a harder Lewis acid than nanosized filler and has a tendency to bond with the hard base in SCN^- to form N-bonded complex, the contact ion-pairs and solvent-separated dimers formed by the interactions of Na^+ with N in SCN^- are the dominant forms of ion association in PEO−NaSCN electrolytes. For this reason, it can be believed that the effect of a nanosized filler on the ion association in PEO−NaSCN electrolytes depends mainly on the balance of interactions of the filler with ether oxygen and with sulfur of SCN^-.

For the FT-IR spectrum of $P(EO)_8NaSCN$ electrolyte, the band at 2037 cm^{-1} is the dominant composition of the spectral envelope for CN stretching modes in the 2150−2000 cm^{-1} region. With the increase of Al_2O_3 content in $P(EO)_8NaSCN$ electrolyte up to 30%, no significant changes are observed for the FT-IR spectrum of PEO and the spectral envelope of SCN^- as shown in Figure 6b. As compared to the XRD pattern of PEO, the XRD pattern of $P(EO)_8NaSCN$, as shown in Figure 7a, exhibits the shift and the changes of relative intensity for two intense peaks of PEO at $2\theta = 19.6°$ and 23.8°. In addition, there are two new peaks that appear at $2\theta = 21.0°$ and 22.2°, and both are associated with the coordination of Na^+ with ether oxygen and the formation of crystalline complex $P(EO)_3NaSCN$.[34] It can be seen from Figure 7 that the XRD patterns of $P(EO)_8NaSCN-Al_2O_3$ composites are almost independent of the filler content and are similar to that of $P(EO)_8NaSCN$. The thermograms are presented in Figure 8 and show that the melting temperature (59.6 °C) of crystalline PEO in $P(EO)_8NaSCN$ electrolytes is similar to those (60.0 °C) in $P(EO)_8NaSCN-10\%Al_2O_3$ and (58.6 °C) in $P(EO)_8NaSCN-30\%Al_2O_3$ composites. All of these experimental results confirm the weak interactions of Al_2O_3 with $(EO)_8NaSCN$ in that the formation of crystalline complex $P(EO)_3NaSCN$ inhibits Al_2O_3 from interacting with ether oxygen. On the other hand, it is shown that the interactions of hard Lewis acid centers on Al_2O_3 surface with the soft Lewis base, sulfur in SCN^-, are so weak that such interactions cannot also cause the disruption of the crystalline complex.

With the increase of Al_2O_3 content in $(EO)_{20}NaSCN$ electrolyte, it is found that the IR spectrum of PEO does not change significantly, and the IR spectrum of PEO in $(EO)_{20}NaSCN-$

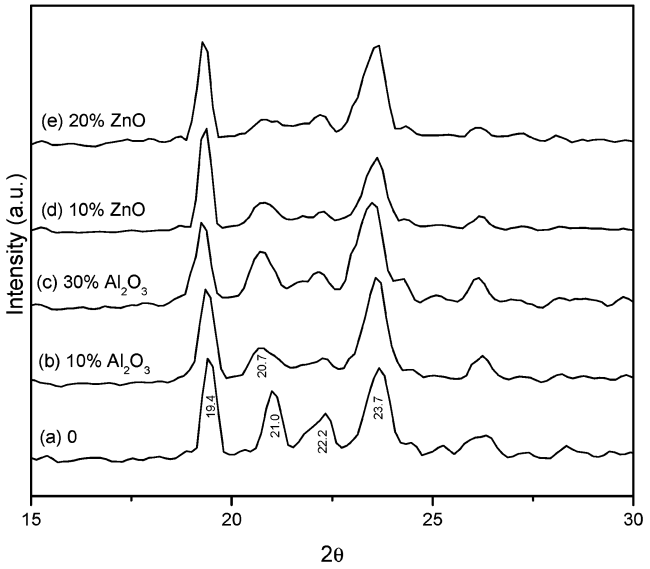

Figure 7. XRD patterns of $P(EO)_8$−NaSCN−Al_2O_3/ZnO nanocomposite electrolytes. Contents for each curve are given as wt % of Al_2O_3/ZnO in PEO.

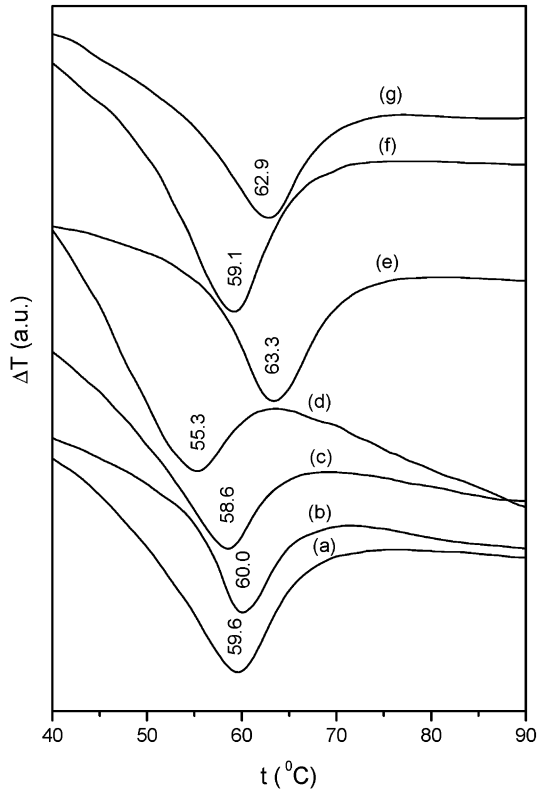

Figure 8. DTA thermograms of PEO−NaSCN−Al_2O_3/ZnO nanocomposites: (a) $P(EO)_8$NaSCN, (b) $P(EO)_8$NaSCN−10%Al_2O_3, (c) $P(EO)_8$NaSCN−30%Al_2O_3, (d) $P(EO)_8$NaSCN−20%ZnO, (e) $P(EO)_{20}$NaSCN, (f) $P(EO)_{20}$NaSCN−10% Al_2O_3, and (g) $P(EO)_{20}$NaSCN−10% Al_2O_3.

Al_2O_3 composites is similar to that in the PEO−20%Al_2O_3 mixture as shown in Figures 1c and 2. However, the addition of Al_2O_3 into $P(EO)_{20}$NaSCN electrolyte can cause the significant changes of the spectral envelop of SCN^- in the range of 2110−2010 cm^{-1} as shown in Figure 9b−d. When Al_2O_3 content in the $P(EO)_{20}$NaSCN electrolyte is less than 10%, the relative intensity of the band at 2037 cm^{-1} increases with an increase of the Al_2O_3 content. When the Al_2O_3 content is increased further, the relative intensity of the band at 2060 cm^{-1}

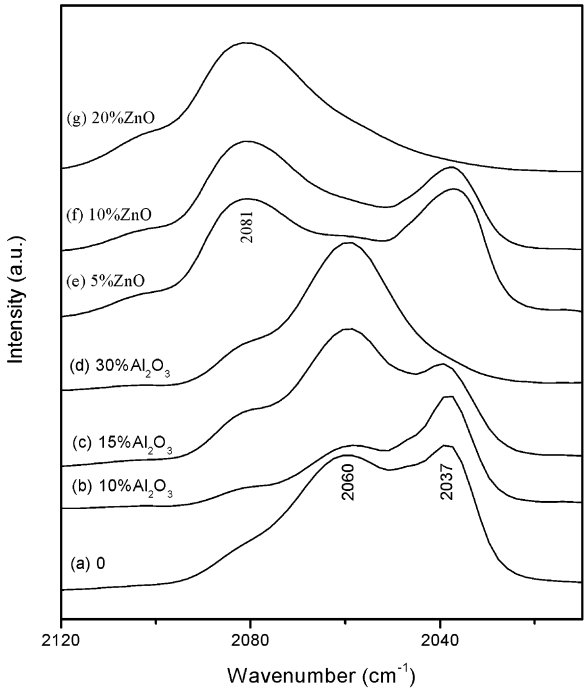

Figure 9. FT-IR spectra of SCN^- in $P(EO)_{20}$−NaSCN−Al_2O_3/ZnO nanocomposite electrolytes in the 2120−2010 cm^{-1} region. Contents for each curve are given as wt % of Al_2O_3/ZnO in PEO.

increases, while that of the band at 2037 cm^{-1} decreases. When the Al_2O_3 content reaches 30%, the band at 2037 cm^{-1} disappears, and the band at 2060 cm^{-1} becomes the dominant composition, which resembles the situation of NaSCN in liquid PEO-250.[30] Although the grain boundary effect of Al_2O_3 is covered by the strong complexation of PEO to NaSCN and cannot be observed from the FT-IR spectrum changes of PEO in the composite, it still occurs when Al_2O_3 is added into $P(EO)_{20}$NaSCN. Because the grain boundary effect can increase the number of trans conformers along PEO chain and repress the solvating ability of PEO toward NaSCN, the content of crystalline complex $P(EO)_3$NaSCN increases with increasing Al_2O_3 content. However, when the Al_2O_3 content in the electrolyte is more than 10%, Lewis acid−base interactions of Al_2O_3 with PEO become significant. Such interactions can transform PEO from crystalline phase to amorphous phase and lead to the disruption of the crystalline complex $P(EO)_3$NaSCN. As a result, the contact ion-pairs and solvent-separated dimers become the dominant forms of ion association.

On the other hand, when the Al_2O_3 content in $P(EO)_{20}$NaSCN electrolyte reaches 30%, the COC stretching mode at 1109 cm^{-1} becomes lightly narrow, and the melting temperature (62.9 °C) of crystalline PEO in the nanocomposite is similar to that (63.3 °C) in $P(EO)_{20}$NaSCN but is higher than that (59.1 °C) in $P(EO)_{20}$NaSCN−10%Al_2O_3 as shown in Figure 8e−g. This suggests that the PEO crystallization induced by Al_2O_3 can still occur on Al_2O_3 surface under the condition of high Al_2O_3 content, even if the solvation of PEO to Na^+ represses the interaction of Al_2O_3 with ether oxygen. Although Al_2O_3 can lead to the polymeric crystallization in the PEO−NaSCN complex, the band at 2037 cm^{-1} disappears only when the Al_2O_3 content is higher than 20%. Therefore, it is suggested that Al_2O_3 can interact not only with ether oxygen in pure PEO, but also with ether oxygen of solvating Na^+. It is expected that the crystalline phase formed by heterogeneous nucleation of Al_2O_3 in $P(EO)_{20}$NaSCN electrolyte contains the contact ion-pairs and solvent-separated dimers. The difference between the crystalline

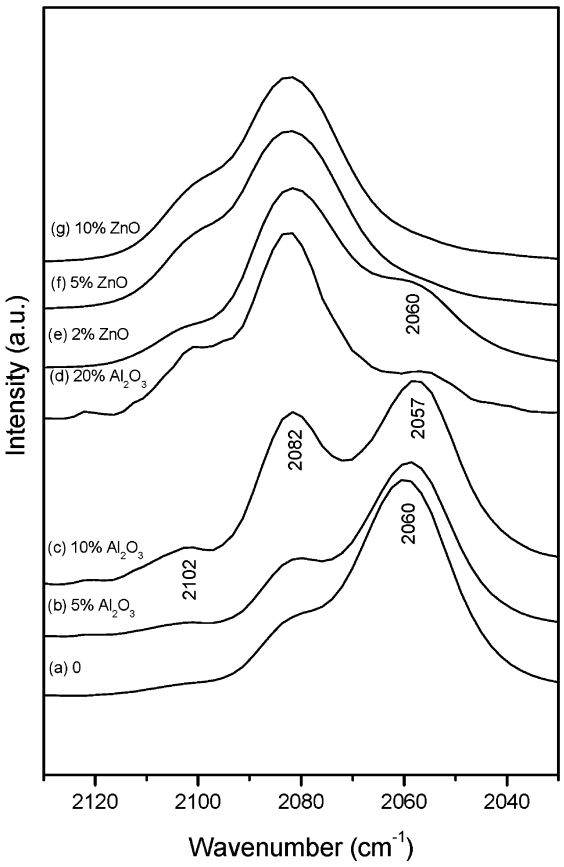

Figure 10. FT-IR spectra of SCN^- in $P(EO)_{60}$−NaSCN−Al_2O_3/ZnO nanocomposite electrolytes in the 2130−2030 cm^{-1} region. Contents for each curve are given as wt % of Al_2O_3/ZnO in PEO.

phase and the PEO−NaSCN complex in the amorphous phase is that the polymeric segment in the former is tightly restricted by the inorganic filler. The interaction of Al_2O_3 with ether oxygen that coordinates with Na^+ can also be observed from the following experimental data.

As shown in Figure 10a, the band at 2060 cm^{-1} in $P(EO)_{60}$-NaSCN electrolyte is the dominant composition of the spectral envelop of CN stretching modes, suggesting that the solvates of PEO and NaSCN are present in the PEO amorphous phase. Therefore, it can be inferred that the forms of ion association do not change due to the transformation of PEO from the crystalline phase to the amorphous phase. However, it is interesting to note that the relative intensity of the band at 2082 cm^{-1} increases, whereas that of the band at 2060 cm^{-1} decreases and disappears finally with increasing Al_2O_3 content. At the same time, the band at 2060 cm^{-1} shifts to 2057 cm^{-1}, and the COC stretching mode at 1110 cm^{-1} in $P(EO)_{60}$NaSCN electrolyte shifts to 1107 cm^{-1} with the increase of Al_2O_3 content. All of these experimental data indicate that the addition of Al_2O_3 into PEO−salt complexes reduces the solvating ability of PEO to NaSCN. There are two possible reasons for this situation: one is the grain boundary effect which brings the disadvantageous condition for the coordination of PEO toward Na^+; another is the Lewis acid−base interaction of Al_2O_3 with the ether oxygen of solvating Na^+ and heterogeneous nucleation of PEO on the Al_2O_3 surface, which produces a poor environment for solvation of PEO toward NaSCN and results in the increase of triple ion aggregation content in PEO−NaSCN electrolytes with low salt contents.

3.3. Interactions of ZnO with PEO−NaSCN Electrolytes. It has been shown that the Lewis acid centers on the ZnO surface are softer than those on the Al_2O_3 surface. Therefore, ZnO will prefer to interact with the sulfur in SCN^- rather than the ether oxygen in PEO−NaSCN electrolytes, and the grain boundary effect can hardly be found in this system. When less than 2% ZnO is mixed with $P(EO)_8$NaSCN electrolyte, the significant change of the spectral envelope in the region of 2150−1950 cm^{-1} is that the band at 2037 cm^{-1} is transformed to 2081 cm^{-1}. The relative intensity of the band at 2081 cm^{-1}, instead of at 2060 cm^{-1}, is strengthened with the disappearance of the band at 2037 cm^{-1} as shown in Figure 6c−e. In PEO−NaSCN and PEO−NaSCN−Al_2O_3 electrolytes, the band at 2081 cm^{-1} is associated with the triple ion aggregations and the poor solvating environment.[18] However, considering the fact that the interaction of ZnO with sulfur in SCN^- is stronger than that with ether oxygen in PEO, the band at 2081 cm^{-1} in PEO−NaSCN−ZnO electrolytes, which increases its relative intensity with increasing ZnO content, is an indication of the complexation of ZnO with S in SCN^- and can be associated with the formation of ZnO···SCN^-. Moreover, this assignment is in good agreement with the analysis on shift of SCN^- complexes.[35,36] Obviously, this situation in PEO−NaSCN−ZnO composites is very different from that found in PEO−NaSCN−Al_2O_3 composites, but similar to that found in PEO−NaSCN−$AlCl_3$ electrolytes which are being investigated in our laboratory. In this system, the interaction of Lewis acid $AlCl_3$ with NaSCN results in the increase of the relative intensity of the band 2081 cm^{-1} and in the formation of $AlCl_3$···SCN^-. These experimental data also indicate that the interaction of ZnO with SCN^- is so strong that it can break up the crystalline complex $P(EO)_3$NaSCN in $P(EO)_8$NaSCN electrolyte. Figure 7d and e shows the XRD patterns of $P(EO)_8$NaSCN−ZnO nanocomposites. Although two intense peaks of PEO at $2\theta = 19.4°$ and 23.7° do not change significantly with the increase of ZnO content in $P(EO)_8$NaSCN, the relative intensities of the peaks at $2\theta = 20.8°$ and 22.2° decrease as a result of the disruption of the crystalline complex caused by the formation of ZnO···SCN^-.

In addition, relative intensities of the bands at 843, 949, and 1360 cm^{-1} increase and the COC stretching and CH stretching modes in the region of 3000−2800 cm^{-1} become broadened when ZnO is added into the electrolyte, suggesting that the big complex anion, ZnO···SCN^-, can play a role of plasticization in $P(EO)_8$NaSCN−ZnO nanocomposites. This fact is also confirmed by the very low melting temperatures (55.3 °C) of crystalline PEO in $P(EO)_8$NaSCN−20%ZnO nanocomposite when compared to that (59.6 °C) in $P(EO)_8$NaSCN electrolyte as shown in Figure 8d. However, the bands of the COC and CH stretching modes will become narrow when the ZnO content in $P(EO)_8$NaSCN is higher than 2%, indicating the presence of the Lewis acid−base interaction of ZnO with PEO. On the other hand, ZnO cannot transform completely the crystalline complex in $P(EO)_8$NaSCN electrolyte into ZnO···SCN^-. This results possibly from the reducing compatablity of ZnO with the SPE as the result of the solvation of PEO to Na^+ and the formation of complex anion.

Figures 9e−g and 10e−g show the changes of the spectral envelope of SCN^- against ZnO content in $P(EO)_{20}$NaSCN and $P(EO)_{60}$NaSCN electrolytes, respectively. The spectral envelope in both systems exhibits a dominant band at 2081 cm^{-1} when the ZnO content is high enough. Moreover, changes of the PEO IR spectrum of both electrolytes against ZnO content are similar to those reported in $P(EO)_8$NaSCN−ZnO nanocomposite. Therefore, it is possible that the same mode of interaction of ZnO with PEO−NaSCN electrolytes occurs in PEO−NaSCN−ZnO composites. Unlike PEO−NaSCN−Al_2O_3 composites, the

salt content in PEO−NaSCN electrolytes exhibits little effect on such a mechanism of interaction between ZnO and PEO−NaSCN electrolytes.

4. Conclusions

Putting all of these pieces together, it is possible to picture the effect of nanosized Al_2O_3/ZnO on the properties of PEO−NaSCN electrolytes. It is noted that the grain boundary effect is an important characteristic of nanosized fillers in PEO. This effect can result in: (1) the decrease of the gauche/trans conformer ratio along the PEO chain, (2) the transform of PEO from crystalline to amorphous phase, (3) the enhancement of the motive performance of PEO segments, and (4) the reduction of the solvating ability of PEO to NaSCN. Therefore, it is expected that the grain boundary effect can promote the ionic transport and improve the conductivity of PEO-based electrolytes, if the salt (such as $LiClO_4$, $LiPF_6$) has difficulty forming a crystal complex in PEO. In addition, Al_2O_3 exhibits a greater grain boundary effect than ZnO, so it has stronger ability to interact with PEO.

Both Al_2O_3 and ZnO are amphotheric oxide and have Lewis acidic centers on their surface. The Lewis acid−base interactions of Al_2O_3/ZnO with ether oxygen can result in the disruption of the PEO crystalline phase. Because the Lewis acidic centers on the Al_2O_3 surface are harder than those on the ZnO surface, the compatibility of Al_2O_3 with PEO is better than that of ZnO, which results in the content of Al_2O_3 in PEO being higher than ZnO when Lewis acid−base interactions become significant. However, the strong interaction of Al_2O_3 with PEO induces the heterogeneous nucleation by the epitaxial effect and promotes the PEO crystallization when the Al_2O_3 content is high enough. It is shown that the surface-induced crystalline phase is different from that of pure PEO, but resembles the amorphous phase in which the segmental motion is confined by the inorganic filler. Therefore, it is expected that the conductivity of PEO-based electrolytes will decrease under such conditions, but the mechanical and thermal stabilities of the bulk phase can be enhanced by this mechanism.

The effect of Al_2O_3 content on the ionic association in PEO−NaSCN electrolytes is related significantly to the salt content due to the strong interaction of Al_2O_3 with ether oxygen. The crystalline complex $P(EO)_3NaSCN$ is the dominant composition in $P(EO)_8NaSCN$ electrolyte, and the weak interaction of Al_2O_3 with S in SCN^- makes it hardly affect the ionic association. When Al_2O_3 is added to $P(EO)_{20}NaSCN$ electrolyte, it can turn the PEO crystalline phase into amorphous phase. As a result, $P(EO)_3NaSCN$ disrupts gradually, and the contact ion-pairs and solvent-separated dimers finally become the dominant components. Although the solvation of ether oxygen to Na^+ represses the interaction of Al_2O_3 with PEO, the crystallization of PEO on the Al_2O_3 surface is also observed in $P(EO)_{20}NaSCN$ electrolyte under the condition of high Al_2O_3 content. Because the contact ion-pairs and solvent-separated dimers are the main compositions in $P(EO)_{60}NaSCN$ electrolyte, the transformation of PEO crystalline phase cannot cause the change of ionic association. However, the interaction of Al_2O_3 with the ether oxygen of solvating Na^+ reduces the solvating ability of PEO to NaSCN and can turn ion-pairs and solvent-separated dimers into triple ion aggregations.

The soft Lewis acidic centers on the ZnO surface exhibit stronger interaction with sulfur in SCN^- than with ether oxygen in PEO−NaSCN electrolytes. This makes the mode of interactions of ZnO with PEO−NaSCN electrolytes almost independent of the salt content. A small quantity of ZnO can significantly turn the ion-pairs, solvent-separated dimers, and even $P(EO)_3NaSCN$ into complex anion $ZnO\cdots SCN^-$, but ZnO cannot disrupt completely $P(EO)_3NaSCN$ in $P(EO)_8NaSCN$ electrolyte because of the solvation of PEO to Na^+ and the formation of complex anion. It is expected that the complexation of ZnO with SCN^- not only possesses the plasticization but also is advantageous in enhancing the cation transport number of SPEs.

Acknowledgment. We wish to acknowledge financial support from the National Natural Science Foundation of China (Grant No. 29973009) and the Innovation Foundation of Henan Education Department.

References and Notes

(1) Dias, F. B.; Plomp, L.; Veldhuis, J. B. J. *J. Power Sources* **2000**, *88*, 169.
(2) Tarasco, J. M.; Armand, M. *Nature* **2001**, *414*, 359.
(3) Henderson, W. A.; Brooks, N. R.; Young, V. G., Jr. *J. Am. Chem. Soc.* **2003**, *125*, 12098.
(4) Azizi Samir, M. A. S.; Alloin, F.; Gorecki, W.; Sanchez, J.-Y.; Dufresne, A. *J. Phys. Chem. B* **2004**, *108*, 10845.
(5) Nishimoto, A.; Agehara, K.; Furuya, N.; Watanabe, T.; Watanabe, M. *Macromolecules* **1999**, *32*, 1541.
(6) Fonseca, C. P.; Neves, S. *J. power sources* **2002**, *104*, 85.
(7) Quartarone, E.; Mustarlli, P.; Magistris, A. *Solid State Ionics* **1998**, *110*, 1.
(8) Azizi Samir, M. A. S.; Alloin, F.; Sanchez, J.-Y.; Dufresne, A. *Macromolecules* **2004**, *37*, 4839.
(9) Bronstein, L. M.; Ashcraft, E.; DeSanto, P., Jr.; Karlinsey, R. L.; Zwanziger, J. W. *J. Phys. Chem. B* **2004**, *108*, 5851.
(10) Croce, F.; Appetecchi, G. B.; Persi, L.; Scrosati, B. *Nature* **1998**, *394*, 456.
(11) Scrosati, B.; Croce, F.; Persi, L. *J. Electrochem. Soc.* **2000**, *5*, 1718.
(12) Croce, F.; Curini, R.; Martinelli, A.; Persi, L.; Ronci, F.; Scrosati, B.; Caminiti, R. *J. Phys. Chem. B* **1999**, *103*, 10632.
(13) Jayathilaka, P. A. R. D.; Dissanayake, M. A. K. L.; Albinsson, I.; Mellander, B.-E. *Electrochim. Acta* **2002**, *47*, 3257.
(14) Croce, F.; Persi, L.; Scrosati, B. *Electrochim. Acta* **2001**, *46*, 2457.
(15) Ji, K.-S.; Moon, H.-S.; Kim, J.-W.; Park, J.-W. *J. Power Sources* **2003**, *117*, 124.
(16) Papke, B. L.; Ratner, M. A.; Shriver, D. F. *J. Phys. Chem. Solids* **1981**, *42*, 493.
(17) Wieczorek, W.; Raducha, D.; Zalewska, A.; Stevens, J. R. *J. Phys. Chem. B* **1998**, *102*, 8725.
(18) Zhang, H.; Xuan, X.; Wang, J.; Wang, H. *Solid State Ionics* **2003**, *164*, 73.
(19) Zhang, H.; Xuan, X.; Wang, J.; Wang, H. *J. Phys. Chem. B* **2004**, *108*, 1563.
(20) Papke, B. L.; Ratner, M. A.; Schriver, D. F. *J. Phys. Chem. Solids* **1981**, *42*, 493.
(21) Aranda, P.; Ruiz-Hitzky, E. *Chem. Mater.* **1992**, *4*, 1395.
(22) Vaia, R. A.; Teukolsky, R. K.; Giannelis, E. P. *Chem. Mater.* **1994**, *6*, 1017.
(23) Wieczorek, W.; Zalewska, A.; Raducha, D.; Florjanczyk, Z.; Stevens, J. R. *J. Phys. Chem. B* **1998**, *102*, 352.
(24) Marcinek, M.; Bac, A.; Lipka, P.; Zalewska, A.; Zukowska, G.; Borkowska, R.; Wieczorek, W. *J. Phys. Chem. B* **2000**, *104*, 11088.
(25) Saito, M.; Ikuta, H.; Uchimoto, Y.; Wakihara, M.; Yokoyama, S.; Yabe, T.; Yamamoto, M. *J. Phys. Chem. B* **2003**, *107*, 11608.
(26) Strawhecker, K.; Manias, E. *Chem. Mater.* **2003**, *15*, 844.
(27) Kulkarni, A. R. *Solid State Ionics* **2000**, *136−137*, 549.
(28) Gadjourova, Z.; Andreev, Y. G.; Tunstall, D. P.; Bruce, P. G. *Nature* **2001**, *412*, 520.
(29) Strawhecker, K.; Manias, E. *Macromolecules* **2001**, *34*, 8475.
(30) Xu, M.; Eyring, E. M.; Petrucci, S. *J. Phys. Chem.* **1995**, *99*, 14589.
(31) Irish, D. E.; Tang, S. Y.; Talts, H.; Petrucci, S. *J. Phys. Chem.* **1979**, *83*, 3268.
(32) Saar, D.; Petrucci, P. *J. Phys. Chem.* **1986**, *90*, 3326.
(33) Bacelon, P.; Corset, J.; de Loze, C. *J. Solution Chem.* **1980**, *9*, 129.
(34) Rhodes, C. P.; Frech, R. *Macromolecules* **2001**, *34*, 2660.
(35) Nakamoto, K. *Infrared and Raman Spectra of Inorganic and Coordination Compounds*; John Wiley and Sons: New York, 1986.
(36) Liu, C.; Teeters, D.; Potter, W.; Tapp, B.; Sukkar, M. H. *Solid State Ionics* **1996**, *86−88*, 431.